Macromolecules

Article

Cite This: *Macromolecules* 2018, 51, 4896−4909

Pressure-Dependent Dynamics of Polymer Melts from Arrhenius to Non-Arrhenius: The Cooperative Free Volume Rate Equation Tested against Simulation Data

Ronald P. White and Jane E. G. Lipson*

Department of Chemistry, Dartmouth College, Hanover, New Hampshire 03755, United States

ABSTRACT: We apply the cooperative free volume (CFV) model to analyze the segmental relaxation times, $\tau(T,V)$, of a model 20-mer polymer melt simulated via molecular dynamics over a broad pressure range. Thermodynamic characterization of the 20-mer allows determination of the constant contribution from the hard-core volume (V_{hc}), which then yields predictions for the free volume, $V_{free} = V - V_{hc}$. The CFV rate model is based on an activation free energy that increases with the number of cooperating segments, n^*, wherein the system's free volume, V_{free}, is what determines n^*. The model predicts that on isotherms ln τ vs $1/V_{free}$ is linear with T-dependent slopes. The 20-mer melt data follow this linear behavior at all temperatures. Assuming a fixed activation energy per cooperating segment leads to a very simple analytic form that describes all of the 20-mer melt's high T behavior, including the Arrhenius to non-Arrhenius transition regime. This form reflects the importance of a gas kinetic contribution as well as both energetic and entropic contributions to the activation energy. Optimization of only one material-dependent parameter leads to collapse of the data. The results of this paper reveal that a key source of non-Arrhenius behavior with decreasing T along isobars is the reduction in V_{free}, which means that segmental rearrangement will require increased cooperativity and higher activation energy. This effect explains the volume contribution to dynamics.

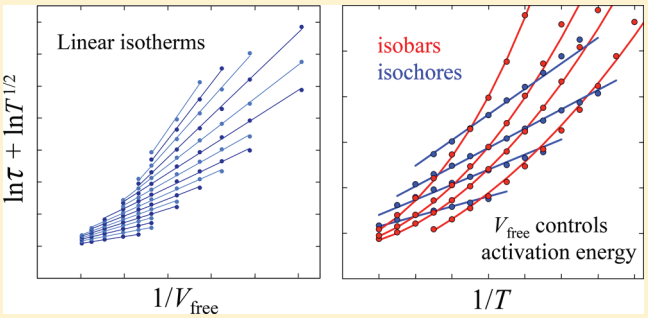

1. INTRODUCTION

A common question in the study of glass-forming liquids relates to why the relaxation dynamics so commonly have apparent activation energies that steadily increase as a melt is cooled toward its glass transition. In other words, why is the behavior non-Arrhenius, and what is driving the activation energy? Here we explore the question of what controls activation energy by applying a new model rate equation, the cooperative free volume (CFV) model, to understand local relaxation processes. With it we can identify several important contributions that drive dynamics over a wide range at high T, including the Arrhenius to non-Arrhenius transition regime. For example, we can show that activation energies are inversely proportional to thermodynamically determined free volume and that over a broad temperature range the latter is, in fact, the very source of non-Arrhenius behavior. Our rate equation was originally applied to simple monomeric fluids; here, we show for the first time that the model accounts for full pressure-dependent dynamics data of a simulated polymer melt.

An important goal in research on molten polymers and other glass-forming liquids has been to explain how their dynamic behavior, e.g., diffusion (D), relaxation times (τ), viscosity (η), etc., depends on their corresponding thermodynamic properties (refs 1−18 provide some examples including background from the point of view of both experiment and models/theory). The common starting point in modeling dynamics and relaxation behavior is the Arrhenius expression, which for τ, is written by

$$\tau = A \exp[B/T] \tag{1}$$

and with analogous expressions, $\eta = A\exp[B/T]$, $D = A\exp[-B/T]$, etc. In eq 1, A is the pre-exponential factor (commonly approximated as a constant), and B is a constant that represents the activation energy. However, as noted above, a hallmark of the behavior of glass-forming liquids is the deviation from eq 1. As T is lowered, plots of ln τ vs $1/T$ become nonlinear, exhibiting upward curvature that indicates an increasing apparent activation energy.

A common practice in working with non-Arrhenius data is to fit it to a well-known phenomenological form, the Vogel−Fulcher−Tammann (VFT) equation[19−21]

$$\tau = A \exp[B/(T - T_0)] \tag{2}$$

This introduces a third parameter, T_0, often called the Vogel temperature. Though the VFT equation can fit data on glass-forming liquids, it is limited in ability to explain the results.

The fact that simple Arrhenius dependence cannot explain the behavior of glass-forming systems has led to the

Received: March 20, 2018
Revised: June 5, 2018
Published: June 18, 2018

DOI: 10.1021/acs.macromol.8b00591
Macromolecules 2018, 51, 4896−4909

consideration of other explanations, some based on free volume[22−25] and some based on entropy.[26,27] The early work for free volume-based approaches started with the "Doolittle equation"[28]

$$\tau = A\ \exp[B/V_{\mathrm{free}}] \tag{3}$$

where V_{free} is the free volume (our own definition for V_{free} is below), and again A and B are typically constants. In historical free volume models, such as those of Cohen and Turnbull (CT)[22] and Williams, Landel, and Ferry (WLF),[24,25] a linear $V_{\mathrm{free}}(T)$ form was substituted into eq 3. This yielded an equation equivalent in form to the phenomenological VFT expression, which does indeed fit super-Arrhenius behavior; however, this does not create a link to any realistic measure of a system's free volume.

In fact, we have shown[29] that when actual *PVT*-based free volumes are used as inputs into eq 3, e.g., on a standard $P = 1$ atm isobar, the resulting dynamics are not correct. In addition, note how eq 3 does not have an explicit temperature dependence; it should fail in situations where the (free) volume is fixed. The notion, as in the Doolittle equation, that free volume alone can explain relaxation behavior does not work. Our own approach features an important role for free volume; we find it to be a key—indeed, a *natural*—variable for understanding relaxation in glass-forming melts, but not the only one.

One of the most influential entropy-based models applied to non-Arrhenius behavior is that of Adam and Gibbs (AG),[26] which describes the rate of segmental rearrangements. In the process, a free energy barrier must be surmounted and this leads to an explicit T dependence (unlike the Doolittle equation). Furthermore, the process is envisioned as requiring a number, z^*, of particles to cooperate. The AG result is given by

$$\tau = A\ \exp\left[\frac{z^*\Delta\mu}{T}\right] = A\ \exp\left[\frac{\Delta\mu s_c^*}{T(S_c/N)}\right] \tag{4}$$

The overall free energy of activation, $z^*\Delta\mu$, is proportional to z^*, where $\Delta\mu$ is the free energy of activation per cooperating particle. The number of cooperating particles, z^*, is determined by the system's average configurational entropy per particle, (S_c/N). That is, $z^* = s_c^*/(S_c/N)$, where s_c^* is the key required amount of configurational entropy that a group must have in order to rearrange. In implementation, S_c is often approximated as the entropy difference between a system's liquid and solid forms;[26,30−33] it can also be computed via simulation techniques.[34−36]

Examples of other models that share connections with the AG model include the cooperative domain model of Matsuaka and Quan[37] and the gear model of Adachi.[38] Both visualize the dynamics in terms of cooperatively rotating groups of conformers and lead to a simple VFT-like T dependence (as do some implementations of the AG model). They can also be applied to analyze the distribution of relaxation times; however, they do not account for pressure dependence of the dynamics, which will be important here.

Many other models exist for describing non-Arrhenius dynamics (see above-cited reviews). For example, mode coupling theory is well-known for predicting a dynamic singularity and the behavior for time correlation functions.[39,40] This is a much more detailed microscopic approach than the CFV model and is based on information from pair density (structural) correlations. Other pair correlation-based approaches include the NLE[41,42] and ECNLE[43,44] theories of Schweizer and co-workers. Though these involve much greater microscopic detail than the CFV model, there are some shared similarities, in the sense that they are both activated rate models that place strong focus on the density dependence of the activation energy.

The cooperative free volume model (CFV) is the approach we will apply here, and some of its attributes are analogous to the basic groundwork laid out in the AG model. To gain a fundamental level understanding, the CFV approach aims for a full pressure-dependent description of dynamics.[1,3] The thermodynamic state of a system is determined by two independent variables, say temperature, T, and volume, V, so it is therefore important to be able to describe how the dynamic response depends on each of these variables independently, i.e., to break down and explain the independent contributions coming from changes in V and those coming from changes in T. The CFV model thus describes $\tau(T,V)$. In contrast, using the VFT expression as an example, note how a single parameter set is not able to describe two different paths through the general *PVT* space, e.g., different isobars, isochores, etc. Treating P-dependent dynamics is much more challenging than modeling just the standard ambient isobar. In addition to the CFV model, there are other treatments that incorporate thermodynamic scaling approaches.[1,3,45−55] These include density scaling, with $\tau = F(TV^{\gamma})$, where F is some unknown function of the single combined variable, TV^{γ}. There are also AG-based[31−33,56] and other entropy-based approaches[46,47] for P-dependent dynamics.

We have found that representing the volume-based contribution to P-dependent dynamics via the system's free volume, V_{free}, is revealing. For instance, in earlier work,[29] we showed for several experimental systems that whenever T is fixed (i.e., on an isotherm), a plot of $\ln\tau$ vs $1/V_{\mathrm{free}}$ produces a linear relationship, with each line having a T-dependent slope. The free volume values that we use are based on analysis of *PVT* data and are obtained completely independently of dynamics experiments. We define V_{free} as the difference between a system's overall volume, V, and its limiting, closely packed, hard-core value, V_{hc}.

$$V_{\mathrm{free}} = V - V_{\mathrm{hc}} \tag{5}$$

This definition is straightforward, though it is important to note that the literature also contains other definitions,[57] such as those that attempt to separate the "total free volume" into "vibrational" and "excess" contributions. Another popular measure of free volume is the Debye−Waller factor, the "rattle space", $\langle u^2\rangle$, swept out by a molecular segment on a picosecond time scale. This quantity is strongly connected to dynamic relaxation[53,58−63] but differs significantly from our V_{free} definition because it can still change with T at constant volume. As eq 5 shows, in our definition V_{free} will only change when there is a change in volume.

The cooperative free volume model (CFV) incorporates both a free volume contribution and an independent temperature contribution in the following general form:

$$\ln\tau = C_1\left(\frac{V_{\mathrm{hc}}}{V_{\mathrm{free}}}\right)\left(1 + \frac{C_2}{T}\right) - \ln T^{1/2} + C_3 \tag{6}$$

Below we show how this form results from making a set of clear physical assumptions. We recently tested eq 6 on a simulated monomeric fluid, the well-studied "KA−LJ" Kob and Anderson

DOI: 10.1021/acs.macromol.8b00591
Macromolecules 2018, 51, 4896−4909

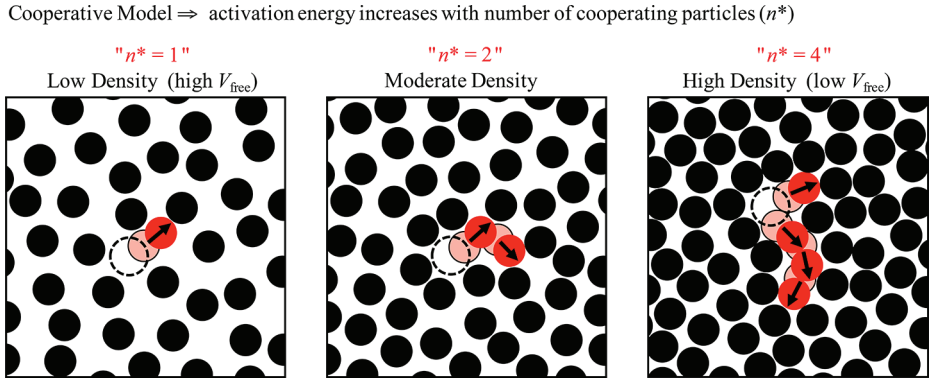

Figure 1. Schematic showing cooperating particles (red), before they make their moves (semitransparent red), and then after (solid red); remaining liquid particles are black. After the moves are made the resulting configuration corresponds to the "activated state" where a full particle-sized vacancy has been created (dashed circle), and once this is formed (or concurrently with its formation), another particle can move into the vacancy to make a full diameter-scale translation and thus escape its previous cage of neighboring particles. As density increases (V_{free} decreases) the number of cooperating particles must increase to make the same-sized vacancy; in this example n^* increases from 1, to 2, to 4. The CFV model activation free energy (ΔA_{act}) depends on n^*: the higher the n^*, the lower the probability of the activated state (P_{act}).

Lennard-Jones mixture,[34−36,64−72] and we showed that it applies well over a broad temperature range including the Arrhenius to non-Arrhenius transition regime.[73] Here we test eq 6 against simulation data extending over a large span of *PVT* space for a bead−spring polymer melt, a common polymer simulation model,[61−63,74] where each polymer molecule is composed of a linear chain of (attractive) Lennard-Jones atoms (segments) held together by the FENE bond potential.

We note that when the temperature is further lowered approaching the system's T_g, the T dependence is not well-described by the above. Instead, the functional dependence on T is well handled using the "thermodynamic scaling" form we previously deduced from studies on experimental P-dependent dynamics of real glass-forming polymer melts:

$$\ln \tau = \left(\frac{V_{hc}}{V_{free}}\right)\left(\frac{T^*}{T}\right)^b + \ln \tau_{ref} \tag{7}$$

Note the gas kinetic $\ln T^{1/2}$ term is not required at low T, and the notation for the parameters (b, T^*, τ_{ref}) comes from that earlier article.[29] Both eqs 6 and 7 can be derived starting from the same CFV model framework, up to the point that produces the general form, $(1/V_{free}) \times f(T)$.[73]

An outline of the remainder of the article is as follows. In section 2, we describe the basic framework of the cooperative free volume rate model. A more detailed derivation is in ref 73. In section 3, we first analyze the *PVT* behavior of the simulated 20-mer fluid, which leads to the evaluation of V_{free} values. Then we compare the behavior predicted by the analytic CFV model $\tau(T,V)$ expression with the actual 20-mer simulation data. Relaxation times are analyzed on isobars, isochores, and isotherms. We discuss the energy and entropy of activation, the importance of the contribution from gas kinetic T dependence, and the role that free volume plays in influencing cooperativity. In this section we also show how free volume connects the appearance of non-Arrhenius behavior with the T-dependent increases in apparent activation energy. In section 4, we provide a summary. A description of the simulation details can be found in the Appendix, as the simulated system and simulation methods used in this work are fairly standard.

2. COOPERATIVE FREE VOLUME MODEL

In this section we describe the CFV rate model. A more detailed description of the derivation is available in ref 73.

The basic molecular level picture of the relaxation event starts by envisioning a liquid particle (or molecular segment) surrounded by other nearby particles, forming a "cage" that restricts movement. We then consider the time that it would take for that particle to move out of the cage of its surrounding neighbors. In order for this to happen, the nearby particles first need to maneuver (redistribute) in such a way that some required amount of free volume, v^*, is gathered on site, creating a new space into which the particle can move. Because sizable spaces are not common in a liquid, we have thus assumed this process must require the cooperation of a number (n^*) of nearby particles such that each one maneuvers to redistribute and consolidate free volume. When these particles have successfully created the required amount of consolidated free space, they have thus adopted a formation that we will call the "activated state". The probability of the activated state is denoted by P_{act}.

A schematic illustration of how this process might work is shown in Figure 1. The positions of the cooperating particles (segments) are shown before they move in semitransparent red, and then after they have moved in solid red. These maneuvers lead to the "activated state", where there is a full particle-sized vacancy (dashed circle) sufficient so that another particle can make a full diameter scale translation and thus escape its previous cage of neighbors. The drawings give a sense for how the number of particles that must cooperate to make the same-sized space is expected to increase with liquid density, and how we quantify this will be described a bit further below.

The overall rate for the relaxation process, R ($\propto 1/\tau$), is given by the following form:

$$R = [\text{constant}] \times T^{1/2} \times P_{act} \tag{8}$$

This is the product of the rate that a particle can cover a distance on the order of its own size (a function of its average gas kinetic velocity), attenuated by the probability, P_{act}, that there is a free space available into which to move. The gas kinetic velocity is proportional to $T^{1/2}$, and the importance of including this contribution was demonstrated for monomeric fluids in ref 73, and we show this to be true here for polymeric

DOI: 10.1021/acs.macromol.8b00591
Macromolecules 2018, 51, 4896−4909

fluids as well. The remaining contributions to the velocity and other directional and geometric considerations associated with the rate process are absorbed into a single constant multiplicative factor denoted by "[constant]".

The probability of the activated state, P_{act}, is given by the following general expression:

$$P_{act} = \exp[-\Delta A_{act}/T] = \exp[-n^*\Delta a/T] \quad (9)$$

ΔA_{act} is the Helmholtz free energy change for the n^* particles to go into their activated state (i.e., to form a space). (The Boltzmann constant has been absorbed for simplicity.) ΔA_{act} comprises the total activation free energy for the process, while $\Delta a = \Delta A_{act}/n^*$ is thus the activation free energy per cooperating particle. In a cooperative model, the activation free energy increases as the number of cooperating particles increase. This structure is embodied by latter form of eq 9.

Since we are interested in understanding relaxation data over a broad temperature range, it is useful to consider a limiting high-T contribution to Δa, entropic in nature and arising due to the molecular hard cores. Thus, we write

$$\Delta a/T = k + \Delta a_{rel}/T \quad (10)$$

where $-k$ is the entropy of activation per cooperating particle; from the approach detailed in ref 73 it follows that k is a positive-valued constant. Δa_{rel} is the value of Δa measured relative to the hypothetical hard-sphere-like state; we refer to Δa_{rel} as the "energy of activation" per cooperating particle and assume that its value is a constant.

Note that ref 73 provides much more detail on the various quantities (k, Δa_{rel}, ΔA_{act}, etc.) defined up to this point.

In the CFV model, the key expectation is that as the free volume in the system decreases, more particles must operate together to open up the required amount of free space, i.e., n^* will increase. We can quantify n^* as follows: In order to be able to make a characteristic-sized space into which a segment can move, we assume that a group of cooperating particles must contain, in total, a characteristic amount of free volume (v^*). It then follows that the group size (the number of cooperating particles, n^*) will be inversely proportional to the overall system's average free volume per particle. That is, n^* is given by

$$n^* = v^*/(V_{free}/N) \quad (11)$$

where N is the total number of particles (segments) in the system. This approach is analogous to the AG framework[26] where the number of cooperating particles, $z^* = s_c^*/(S_c/N)$, is inversely proportional to the configurational entropy per particle. (In ref 57 we have discussed the connection between free volume and entropy.) Our assumption that v^* is constant is thus similar to the AG assumption that the configurational entropy in a cooperating group (s_c^*) is constant. In our case, as V_{free} decreases there should be an increase in n^*, leading to the relationship $n^* \propto 1/V_{free}$, and this form will dictate the activation free energy.[29,73]

Substituting eqs 10 and 11 into $P_{act} = \exp[-n^*\Delta a/T]$ (eq 9), and using this in the rate equation, $R \propto 1/\tau \propto T^{1/2}P_{act}$ (eq 8), leads to the main result, eq 6 above. Equation 6 is written in terms of the convenient working measure of relative free volume, V_{hc}/V_{free}. The three system-dependent parameters are $C_1 = kv^*/(V_{hc}/N)$, $C_2 = \Delta a_{rel}/k$, and C_3 (related to the system-dependent limiting behavior). We will apply eq 6 with fixed constant values for C_1, C_2, and C_3 because we have assumed v^*, k, and Δa_{rel} to each be constants.

We emphasize that a system's T- and P-independent V_{hc} value is determined *a priori*, from the *PVT* analysis, independent of any dynamics data. We have noted in refs 29, 57, and 73 that historical free volume models have free volume values that have been fit to produce results that match relaxation data, and those values are therefore not necessarily consistent with experimental volumes. This cannot happen in the CFV model.

Equation 6 expresses relaxation times as a function of two *independent* thermodynamic variables, T and V_{free}, or equivalently, T and V. It will describe $\tau(T,V)$ for all points within a range of general T,V space (any general path) with just a *single set* of model parameters. This is a much more demanding test than the typical scenario of restricting a model's application to $\tau(T)$ on the P = 1 atm isobar.

3. RESULTS AND DISCUSSION

In this section the CFV model is applied to analyze simulation results for the 20-mer bead−spring polymer fluid. In the simulations, each polymer molecule comprises 20 Lennard-Jones (LJ) atoms (segments) with bonded connections described by the FENE potential; in all cases, the fluid systems consisted of 80 molecules and thus a total of $N = 80 \times 20 = 1600$ LJ atoms (segments). Molecular dynamics simulations were carried out under standard periodic boundary conditions to obtain average thermodynamic properties and the corresponding segmental relaxation times, τ. The latter is a measure of the time for segments to move distances on the order of their own size and is defined by the time of decay in the self-intermediate scattering function, $F_s(q,t)$. Note that for all T, V conditions we have chosen the same value of $q = 7.07\sigma^{-1}$. This value is close to the first peak in the (intermolecular) structure factor $S(q)$; however, the peak does depend on density. Using the same q value results in relaxation times that are defined for a consistent characteristic distance. For conditions at high T and low density, the distinction between "vibration" and "breaking free from a cage" becomes less clear, so the reported τ values will thus simply represent the degree of segmental movement. This choice also leads to clarity in the role of the gas kinetic contribution, such that a simplifying low-density convergence point for relaxation times is obtained (results below) where only the gas kinetic prefactor determines the "relaxation time". In the results, all quantities will be reported in standard LJ units where length is in σ, energy in ε, time in $\sigma(m/\varepsilon)^{1/2}$, etc., where m is the atom (segment) mass and σ an ε are the LJ distance and energy parameters. Full simulation details are in the Appendix.

3.1. *PVT* Behavior and Limiting Hard-Core Volume.

In order to implement the CFV model for the dynamics, we first perform an analysis of the system's pressure−volume−temperature (*PVT*) behavior; this will lead to thermodynamic values for the system's free volume at any desired point. Using our definition for free volume, $V_{free} = V - V_{hc}$ (eq 5), requires the value of V_{hc}. We will follow the approach we used for the KA−LJ monomer fluid in ref 73, where we extrapolated the limiting hard-core volume from plots of the *PVT* data.

Figure 2 shows the results for the 20-mer fluid *PVT* behavior in the form of $V(T)$ isobars. As was the case for the monomer fluid in ref 73, a reasonable estimate of the system's limiting hard-core volume, V_{hc}, can be made just from simple visual inspection of the $V(T)$ curves because the range of *PVT* space shown here is quite large. Dashed lines for each isobar have been drawn as a guide to the eye that extend from the

DOI: 10.1021/acs.macromol.8b00591
Macromolecules 2018, 51, 4896−4909

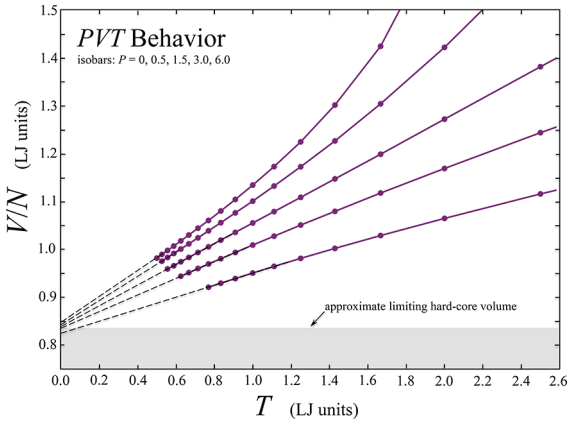

Figure 2. *PVT* behavior for the 20-mer polymer fluid. Shown are results for V/N as a function of T for isobars of P = 0, 0.5, 1.5, 3.0, and 6.0. Values are in standard LJ units. V/N is the volume per LJ atom (segment). Extrapolations (dashed lines) are drawn as a guide to the eye in approximating the system's limiting close-packed, hard-core volume, $V_{hc}/N \approx 0.84$, which is used in the free volume calculations, $V_{free} = V - V_{hc}$.

simulation data down to V at T = 0. Having curves for several isobar pressures (covering the P range of interest) is helpful in bracketing some reasonable bounds around a good average estimate, here about V_{hc}/N = 0.83 to 0.85. This range of uncertainty has little effect on the analysis (see the detailed tests in ref 73). We will take V_{hc}/N = 0.84 as the limiting hard-core volume and use this single value throughout the paper. To put the physical meaning of this limiting volume in context, consider the packing fraction of equal spheres, $(\pi/6)/(V/N)$. Random close-packing of such a liquid corresponds to a packing fraction of 0.64. The limiting segment packing fraction here for the 20-mer fluid is fairly close, with a value of $(\pi/6)/(0.84)$ = 0.62. A connection between the limiting volume, V_{hc}, and the condition of random close packing was also shown in ref 73 for the monomeric KA–LJ mixture.

3.2. *T* Dependence of Relaxation Data: Accounting for the Contribution from the Average Kinetic Gas Velocity.

The CFV rate model begins with a familiar Arrhenius-type exponential contribution that brings in the activation energy for the process ($P_{act} = \exp[-\Delta A_{act}/T]$, eq 9); however, the overall rate eq 8 includes a T-dependent prefactor as well. The contribution from the average gas kinetic velocity is expected in the prefactor, but it is often ignored because its temperature dependence ($T^{1/2}$) is anticipated to be much weaker than that arising from the T dependence of the exponential term. However, if the value of the system's activation energy is not large enough for the exponential to strongly dominate the prefactor (say, when T is doubled or more in the high-T regime), then failing to account for the $T^{1/2}$ dependence may be consequential. In order to illustrate this we will consider first raw simulation data plotted as a series of isochores; we will then turn to isobars.

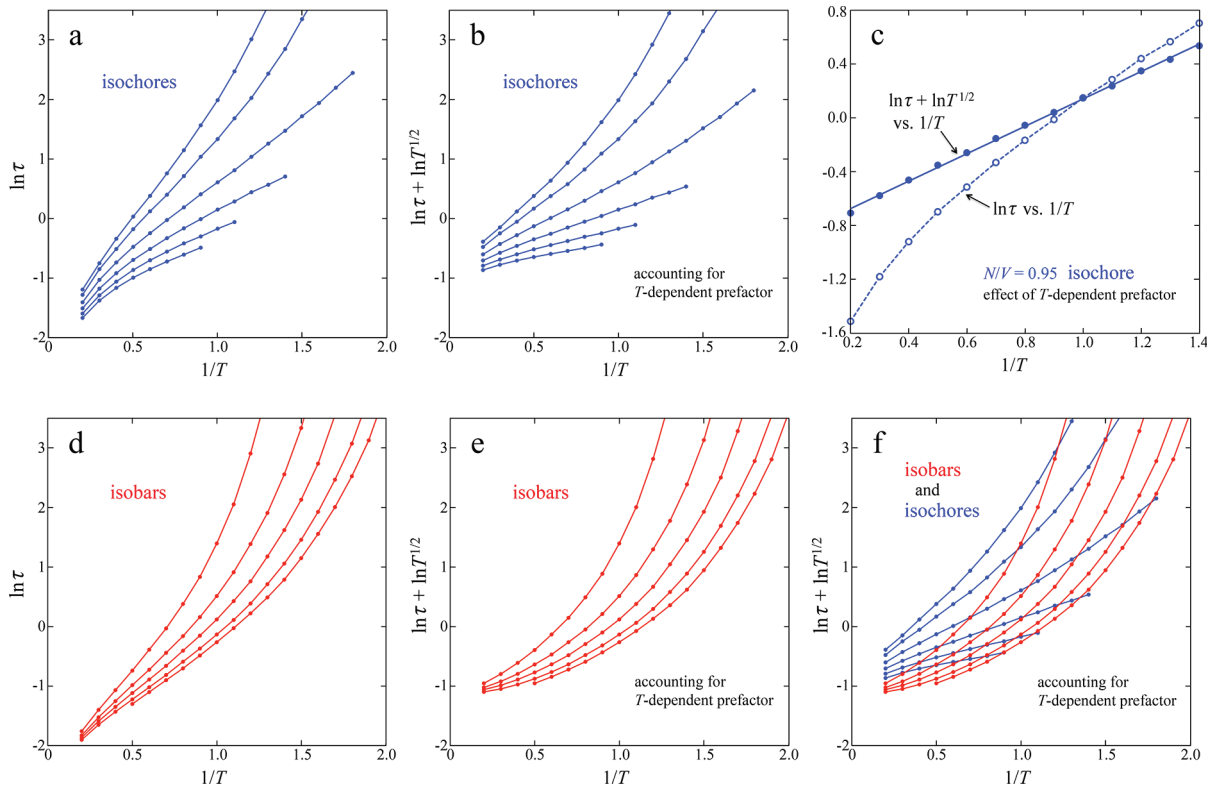

Figure 3. Simulation data for the 20-mer polymer fluid: relaxation times on isobars and isochores. Panel "a" shows ln τ vs $1/T$ isochores with densities, N/V = 0.85, 0.90, 0.95, 1.00, 1.05, and 1.08. Panel "b" shows the same results plotted as ln τ + ln $T^{1/2}$ vs $1/T$ which adjusts for the T dependence of the gas kinetic velocity in the pre-exponential factor. Panel "c" shows a close-up of the N/V = 0.95 isochore plotted with and without the adjustment. Isobars are plotted as ln τ vs $1/T$ in panel "d" and as ln τ + ln $T^{1/2}$ vs $1/T$ in panel "e"; the isobar pressures are P = 0, 0.5, 1.5, 3.0, and 6.0. Panel "f" shows the isochores and isobars together, plotted in the adjusted ln τ + ln $T^{1/2}$ vs $1/T$ form. Values are in LJ units. Note the termination of some of the isochores at low T (high $1/T$) is due to cavitation (negative P), and the P = 0 isobar terminates at high T due to evaporation.

DOI: 10.1021/acs.macromol.8b00591
Macromolecules 2018, 51, 4896–4909

In Figure 3a, the simulation results obtained for the segmental relaxation times (τ) of the 20-mer fluid are plotted as ln τ vs $1/T$ in the form isochores. The densities (N/V) are 0.85, 0.90, 0.95, 1.00, 1.05, and 1.08. Details on calculating τ, a measure of the time for segments to move distances on the order of their own size, are in the Appendix. At high T (low $1/T$), linear plots are expected, reflecting the so-called Arrhenius regime. However, in Figure 3a the plots show clear downward curvature as high T is approached. Contrast these with the plots shown in Figure 3b, where we account for the T-dependent contribution to the prefactor by removing it, i.e., by plotting ln τ + ln $T^{1/2}$ vs $1/T$. Now in the high-T region the plots are indeed linear and confirm the expectation that Arrhenius-type behavior (constant apparent activation energy) is occurring. This is shown even more clearly in Figure 3c, wherein a single isochore (N/V = 0.95) is plotted with and without the kinetic gas correction.

The slopes for the linear set of plots shown in Figure 3b can be used to determine the activation energies. Comparing the set of isochores in Figures 3a and 3b, it is also clear that there is a significant change in the average slopes in the high-T regime; in fact, the corrected (Figure 3b) activation energy is typically about half the value of the estimate without the correction (Figure 3a). Not accounting for the gas kinetic correction will not only lead to inaccurate estimates of the activation energy but will also incorrectly estimate the extent to which the activation energies change as a function of density.

In Figures 3d and 3e the simulation results obtained for the segmental relaxation times (τ) of the 20-mer fluid are plotted in the form of isobars having P = 0, 0.5, 1.5, 3.0, and 6.0. Figure 3d shows the results without the kinetic correction in the prefactor, which is then accounted for in Figure 3e to the right. The high-temperature downward curvature that was particularly evident for the case of the isochores is visible in the ln τ vs $1/T$ isobars, but to a much lesser degree. Instead, it is the Figure 3e ln τ + ln $T^{1/2}$ vs $1/T$ plots that show stronger curvature, in this case, an enhancement of the upward curvature.

Compared to the isochores, the uncorrected isobars do appear to exhibit a degree of linearity at high T, but does this mean that accounting for the T dependence of the prefactor has become less important? That cannot be a sensible conclusion, since its functional contribution should not depend on how the data are plotted. If we are to conclude that the gas kinetic correction matters for isochores, then we must also argue its importance for isobars.

In fact, the appearance of linearity in the uncorrected ln τ vs $1/T$ isobars is explained by the underlying density-driven changes in the activation energies (ΔA_{act} increasing as $V(T)$ decreases). This effect, reflected in the clear positive curvature of the isobars (a form predicted by CFV below), partially cancels with the inherent negative curvature of the gas kinetic T dependence to produce the appearance of linearity. However, the cancellation is effective only over a limited T-range because even at high T, if T is further increased, the downward curvature on the ln τ vs $1/T$ isobars will reappear. As noted, this can be seen in Figure 3d and is very clear in Figure 4 of ref 73 in our study of monomers.

We expect that the effect of the gas kinetic T dependence should be important in most simulation investigations because, although simulations probe non-Arrhenius behavior, they still tend to be restricted to a regime of relatively high T such that changes in $T^{1/2}$ are competitive with those in $\exp[-\Delta A_{act}/T]$. By comparison, experimental dielectric spectroscopy studies probe in a range such that T typically varies between T_g and (roughly) $\sim 1.3T_g$. Under those conditions the effective activation energies are much higher, driving much stronger changes in τ, while the changes in the gas kinetic contribution are small by comparison.

3.3. Volume Dependence of Relaxation Data: Free Volume Is a Natural Variable. The CFV model expression eq 6 predicts that isothermal changes in ln τ are expected to be linearly proportional to inverse free volume and that the isotherm slopes should increase as the temperatures decrease. We test this key prediction against the simulation results in the upper panel of Figure 4 where ln τ vs V_{hc}/V_{free} is plotted for multiple isotherms. As expected, all the isotherms display clear linearity, and the slopes systematically increase with decreasing T. This behavior was initially shown in experimental data on glassy melts[29] and more recently in the simulations of the simple KA–LJ monomeric liquid in ref 73; results for the latter are included as an inset in the figure. Here we demonstrate for the first time linear isothermal ln τ vs V_{hc}/V_{free} behavior for a simulated polymer melt.

These results make a strong case for the linkage of free volume with dynamic behavior because in our treatment the dynamics data are not used in predicting values for the free volume. The limiting hard-core volume value (V_{hc} = 0.84) that leads to $V_{free} = V - V_{hc}$ was obtained by analyzing the 20-mer melt's PVT behavior. The abscissa values for each point are therefore calculated using only thermodynamic quantities. Here it is also worthwhile to add that any uncertainty in the V_{hc} value does not lead to any significant change in the results (e.g., see detailed tests in ref 73 and footnote 75).

We argued above for the importance in accounting for the $T^{1/2}$ dependence of the prefactor, so the lower panel of Figure 4 shows ln τ + ln $T^{1/2}$ vs V_{hc}/V_{free} plotted as isotherms; the effect is a shift in the intercept of each linear isotherm. These results now show there to be a clear convergence pattern to a limiting value at high V_{free} (low $1/V_{free}$), and thus the "fan-like" pattern of ln τ + ln $T^{1/2}$ vs V_{hc}/V_{free} lines radiates from this point. Equation 6 predicts a convergence point at high V_{free}, as it is embodied in the limiting constant C_3. When plotted in the ln τ + ln $T^{1/2}$ vs V_{hc}/V_{free} form, the convergence shows that at low density the gas kinetic velocity should be the only important T-dependent contribution in determining the time for a particle to traverse a distance on the order of its own size. This form of plotting the isotherms also emphasizes how the remaining T dependence (the $(1 + C_2/T)$ term in eq 6) is the key part that serves in making the isotherm slopes systematically increase with decreasing T.

3.4. Parametrization of the Cooperative Free Volume Model. We next turn to fitting the $\tau(T,V_{free})$ simulation data in order to obtain values for the system-dependent parameters C_1, C_2, and C_3. Although all three parameters can be determined at once, here we do the fit in two stages (determining the C_2 parameter first) because it is useful in discussing the features of eq 6. We focus on just the high-T half of the set of isotherms in Figure 4, choosing $1/T$ = 0.2 through 1.1. As noted in the Introduction, eq 6 does eventually break down at low T; a fit to the higher T data, alone, will allow us to probe (in section 3.5) how far into lower T the eq 6 form continues to hold. The choice of low T cutoff of $1/T$ = 1.1 represents roughly the average temperature at which the isochores become nonlinear in Figure 3b.

DOI: 10.1021/acs.macromol.8b00591
Macromolecules 2018, 51, 4896–4909

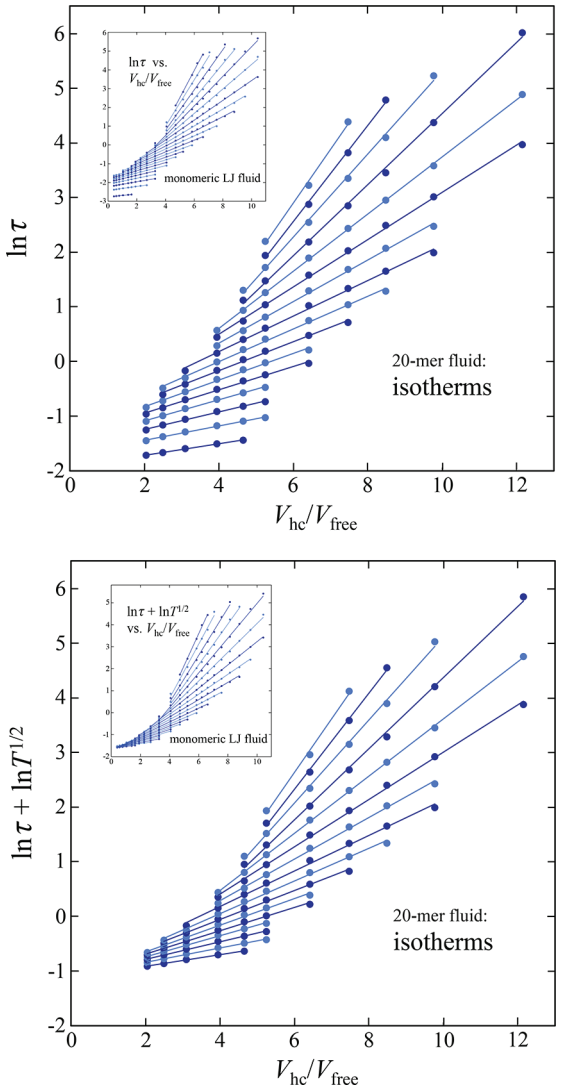

Figure 4. Linearity in (log of) relaxation times as a function of inverse free volume on isotherms of the 20-mer polymer fluid. The upper panel shows ln τ vs V_{hc}/V_{free} for isotherms of $1/T$ = 0.2 to 1.7 in increments of 0.1. Values are in standard LJ units. Pressure values on each isotherm typically range from P = 0 up to values of about 7 to 9. (P values range even higher for high T isotherms ($1/T$ < 0.5), while the highest P's are lower for low-T isotherms ($1/T$ > 1.4) due to run length limitations for sampling large τ values.) The lower panel shows the same isotherms plotted as ln τ + ln $T^{1/2}$ vs V_{hc}/V_{free}, where adding the ln $T^{1/2}$ term on the ordinate demonstrates the effect of adjusting for the T dependence coming from the gas kinetic velocity (pre-exponential factor contribution). The insets show the corresponding linear trends obtained for the monomeric KA–LJ fluid in ref 73 for isotherms ranging from $1/T$ = 0.1 to 2.1 (full details available in ref 73).

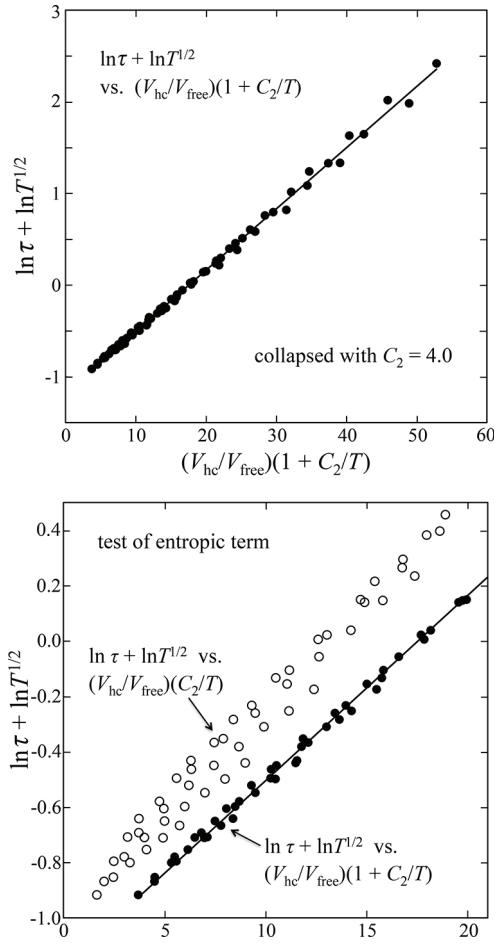

Figure 5. Application of the CFV model eq 6 to 20-mer melt relaxation behavior. To parametrize the model, plots here consider the results coming from ten of the isotherms in Figure 4, $1/T$ = 0.2 to 1.1 in increments of 0.1. The upper panel shows a plot of [ln τ + ln $T^{1/2}$] vs [$(V_{hc}/V_{free}) \times (1 + C_2/T)$] (linear variables from eq 6); here the data have been collapsed into a single line with a choice of C_2 = 4.0. (The activation energy per cooperating particle is proportional to C_2.) The data collapse demonstrates that the eq 6 form is correct. The slope and intercept of the collapsed line lead directly to the values for the remaining parameters, C_1 = 0.0669 and C_3 = −1.173. The lower panel is a comparison showing that a collapse is not obtained when the entropic unity term is removed in a plot of [ln τ + ln $T^{1/2}$] vs [$(V_{hc}/V_{free}) \times (C_2/T)$], wherein, no value of C_2 can collapse the high T data; C_2 = 4.0 is shown.

Equation 6 predicts a linear relationship between the variables [ln τ + ln $T^{1/2}$] and [$(V_{hc}/V_{free}) \times (1 + C_2/T)$]. If this form is correct, then there should be a choice for C_2 that will collapse the data from the multiple isotherms into a single straight line. In the upper panel of Figure 5, we show a plot of ln τ + ln $T^{1/2}$ vs $(V_{hc}/V_{free}) \times (1 + C_2/T)$ that demonstrates this collapse, using a value of C_2 = 4.0 determined by trial and error adjustment. The sensitivity of the collapse to the choice of C_2 is about ±0.3 (see note 76). The "second stage" of the fit follows immediately because the form is linear. The remaining parameters, C_1 = 0.0669 and C_3 = −1.173, are set once C_2 is fixed because they correspond to the line's slope and intercept, respectively. The quality of the data collapse demonstrates that eq 6, with a constant C_2, does a very good job of matching the system's dynamics behavior. This provides support for the view that there is a constant amount of activation energy accrued for each cooperating segment that participates. (As described in section 2, the activation energy per cooperating segment is proportional to C_2 and, technically, also to C_1; both C_1 and C_2 are constant.) The collapsed isotherms correspond to a wide range of T and P, and additional plots showing a variety of paths through PVT space (e.g., isobars and isotherms) will be shown below.

Recall that the unity in the factor $(1 + C_2/T)$ in eq 6 traces back to the entropic contribution to the activation free energy per cooperating segment. This is a contribution that persists

DOI: 10.1021/acs.macromol.8b00591
Macromolecules 2018, 51, 4896–4909

into high T due to the effect of lingering segmental hard cores (an athermal effect).[77] The set of open symbols in the lower panel of Figure 5 illustrates what happens if we fail to account for this contribution: the data, especially those toward the higher T end, do not collapse. There is no choice of value for C_2 that can collapse the data in a plot of $\ln \tau + \ln T^{1/2}$ vs $(V_{hc}/V_{free})(C_2/T)$; changing C_2 will only shift the numerical values on the x-axis ($C_2 = 4.0$ is shown). These results demonstrate that the entropic term present in the form of eq 6 does in fact play an important role and that both entropic and energetic contributions need to be accounted for.

The importance of accounting for an entropic contribution was a conclusion also reached by Betancourt et al.[61] These authors used their polymer simulation data and compared relaxation times with corresponding results from a direct counting method for numbers of cooperating segments. In fact, there have been different attempts to track and quantify the numbers of cooperating particles via simulation-based counting methods, correlation functions, and related quantities (refs 61 and 74 are a couple of examples). Of course, any such method requires choices in defining what qualifies as an "observed cooperating group". The present CFV quantification can only elucidate such numbers to within a proportionality constant; however, it is still useful to compare other types of estimates with the present thermodynamic V_{free}-based trends.

Note that the eq 6 parameters have sensible values: The energetic parameter, $C_2 = \Delta a_{rel}/k = 4.0$, is on the scale of the LJ pair interaction energy ($\varepsilon = 1$). The volume-related parameter, $C_1 = kv^*/(V_{hc}/N) = 0.0669$, is also on the scale of the 20-mer liquid's typical relative free volume values (e.g., V_{free}/V_{hc} values around 0.1 are typical at $P = 6$). Furthermore, multiplying C_1 and C_2 (to eliminate k) gives an "energy-volume value" of $C_1C_2 = v^*/(V_{hc}/N)\Delta a_{rel} = 0.27$, which is on a similar scale to the product of the LJ interaction energy ($\varepsilon = 1$) multiplied by a typical system V_{free}/V_{hc} value. For the case of the KA–LJ monomeric fluid,[73] we obtained a value of $C_2 = 3.0$ (LJ units). Here, the $C_2 = 4.0$ value sensibly reflects the likelihood that the activation energy for relaxation of segments in a polymer chain would be higher than that for free segments. The KA–LJ value of $C_1 = 0.0719$ is fairly close to the present 20-mer value of 0.0669.

In addition, it is illuminating to compare the balance between the entropic and energetic contributions to the activation energy. As noted above, the entropic term is represented by the "reduced value" of unity (with k divided out); the energetic term is C_2/T. In going from high T (say $1/T = 0.2$) to lower T ($1/T = 1.1$), C_2/T (with $C_2 = 4.0$) varies from 0.8 to 4.4. At the highest T the entropic term is comparable to the energetic term; however, at the lowest T in this range it becomes 4.4 times weaker than the energetic term. Over this T range there is a notable shift in the entropy–energy balance in eq 6.

3.5. Discussion of Results Using the Cooperative Free Volume Model. Having discussed the volume and temperature contributions to relaxation behavior, as well as the constants, that comprise eq 6, we now turn to analyzing the relaxation time behavior on isobars. This is a particularly strong test for the form of the CFV model because on an isobar T and V are changing simultaneously. We will focus initially on a single isobar for the 20-mer melt, $P = 3$, shown in Figure 6 where $\ln \tau + \ln T^{1/2}$ is plotted against $1/T$. The points correspond to the simulation data, and the curve corresponds to eq 6 (same parameters as in the discussion above: $C_1 = 0.0669$, $C_2 = 4.0$, $C_3 = -1.173$).

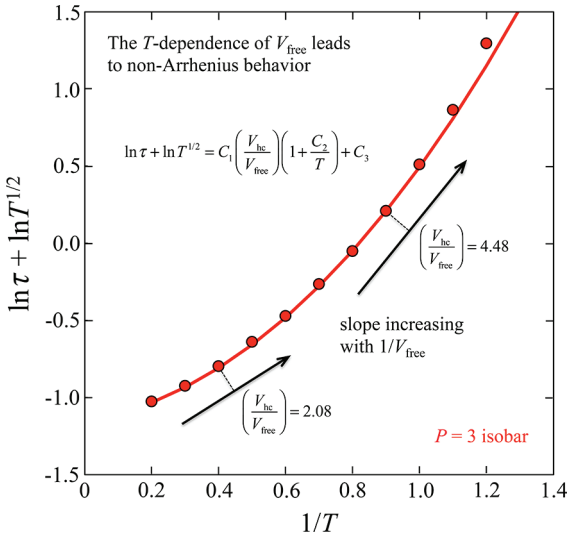

Figure 6. Application of the CFV model to 20-mer relaxation behavior: $[\ln \tau + \ln T^{1/2}]$ vs $1/T$ on the $P = 3.0$ isobar. The curve corresponds to model eq 6, $\ln \tau = C_1(V_{hc}/V_{free}) \times (1 + C_2/T) - \ln T^{1/2} + C_3$, with parameters $C_1 = 0.0669$, $C_2 = 4.0$, and $C_3 = -1.173$; the points are the simulation data. The model captures the non-Arrhenius behavior along the isobar because the increasing $1/V_{free}$ (increasing with $1/T$) causes an increase in the overall activation free energy ($\Delta A_{act} = n^*\Delta a$). The model interpretation is that the increasing $1/V_{free}$ causes an increasing number of cooperating segments, $n^* \propto 1/V_{free}$. (Note this increase in ΔA_{act} occurs while the activation energy *per cooperating segment* (C_2) remains constant.) Along the isobar, two points are marked to illustrate where $1/V_{free}$ (and thus n^*) has changed by roughly a factor of 2, and with this, there is the clear increase in the apparent activation energy (slope). (Note that ΔA_{act} and the slope, $(\partial[\ln \tau + \ln T^{1/2}]/\partial(1/T))_P$, are closely linked to each other but technically not mathematically identical.)

The form of the curve predicted using eq 6 compares well with the simulation data; we note that both data and model reveal behavior that is very clearly non-Arrhenius. The substantial upward curvature in the isobar plot means that the apparent activation energy is increasing with decreasing T. The CFV model explains why this should happen.

On an isobar, as T decreases, V_{free} is also decreasing. In terms of the CFV picture, this means that the number of cooperating particles is increasing ($n^* \propto 1/V_{free}$), which causes an increase in the total activation free energy ($\Delta A_{act} = n^*\Delta a$). As an illustrative example, Figure 6 shows the difference between two selected points on the isobar. The value of V_{hc}/V_{free} ($\propto n^*$) changes significantly, going from 2.08 to 4.48, and associated with this is the dramatic change in the apparent activation energy; the slope of the isobar roughly doubles between those two points. (Note the activation free energy, ΔA_{act}, and the "apparent activation energy", defined by the slope, $(\partial(\ln \tau + \ln T^{1/2})/\partial T^{-1})_P$, are closely linked to each other, but they are not mathematically identical.)

The above explains the way in which non-Arrhenius behavior is driven by the free volume effect: the activation energy per cooperating segment (C_2) is constant, so a changing $1/V_{free}$ is the only way to drive up the total activation energy. Looking directly at the form of eq 6, it is evident that a plot of $(1/V_{free}) \times (1 + C_2/T)$ vs $1/T$ must result in upward curvature because $1/T$ and $1/V_{free}$ are both increasing on an isobar. Put simply, isobars are non-Arrhenius because $(1/V_{free}) \times (1/T)$ rises faster than $1/T$.

DOI: 10.1021/acs.macromol.8b00591
Macromolecules 2018, 51, 4896–4909

The same single CFV model parametrization applies over a wide (T, V, P) space. Figure 7 shows several isobars and isochores plotted again as $\ln \tau + \ln T^{1/2}$ vs $1/T$. Isobars are for P = 0, 1.5. 3.0, and 6.0, and isochores are for density (N/V) values of 0.80, 0.90, 0.95, and 1.00. The points are the simulation data, and the curves correspond to eq 6 with the same C_1, C_2, and C_3 values as above. We note that although these constants were obtained by fitting the range of $1/T$ = 0.1−1.1 the model curves are in good agreement with the simulation data extending through values of $1/T$ = 1.2−1.4 and even to 1.6 at low P. At low enough T the agreement is expected to break down, and the start of this is visible for the very lowest temperatures on each isobar and on the highest density isochore. This eventual breakdown is also seen in the monomeric results as well, and thus is not a result specific to the intramolecular energetic barriers of the polymer model. How the model may be applied to low temperature behavior is discussed below.

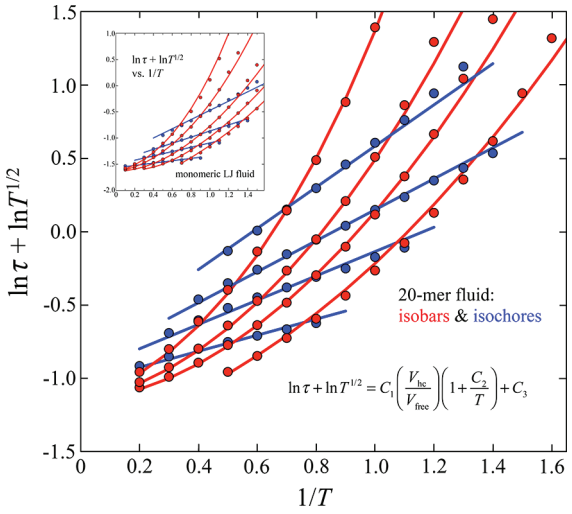

Figure 7. Application of the CFV model to 20-mer relaxation behavior over a broad PVT space: $[\ln \tau + \ln T^{1/2}]$ vs $1/T$ for multiple isobars and isochores. The curves correspond to the CFV model eq 6, $\ln \tau = C_1(V_{hc}/V_{free}) \times (1 + C_2/T) - \ln T^{1/2} + C_3$, with parameters C_1 = 0.0669, C_2 = 4.0, and C_3 = −1.173; the points are the simulation data. Isobars, in red, from bottom to top, are for P = 0.0, 1.5, 3.0, and 6.0. Isochores, in blue, bottom to top, are for density (N/V) = 0.80, 0.90, 0.95, and 1.00. Values are in LJ units. The inset shows the corresponding application of model eq 6 to the monomeric KA−LJ fluid (see ref 73), where C_1 = 0.0719, C_2 = 3.0, and C_3 = −1.644, and shown are isobars of P = 0.5, 1.5, 3.0, 6.0, and 9.0 and isochores of N/V = 0.70, 0.90, 1.00, and 1.10.

Over the wide range of higher T's, the apparent activation energy, $(\partial(\ln \tau + \ln T^{1/2})/\partial T^{-1})_V$ (i.e., the slope), is constant on any single isochore. Its value depends sensitively on the isochore density, and these changes follow from the connection to V_{free}, viz. $\Delta A_{act} = n^*\Delta a$, where $n^* \propto 1/V_{free}$. As Figure 7 shows, the CFV model eq 6 gets this right, accurately capturing that increasing density requires more segments to participate in creating an available space for local motion, leading to an increase in the activation energy and thus an increase in slope.

Turning to the set of isobars, the CFV model clearly captures the non-Arrhenius behavior at each value of P, showing the anticipated change in steepness from one isobar to the next. In addition, starting from the same T, V point the isobars in Figure 7 rise more steeply than isochores. The apparent activation energy remains constant for the isochore but will consistently increase along the isobar, since the increasing slope is driven by the changes in V_{free}, as discussed above.

It is important to note that eq 6 applied equally well to the KA−LJ monomeric fluid studied in ref 73 as it has applied to the 20-mer melt studied here; the inset to Figure 7 shows the monomer results. This confirms the role of free volume as a natural variable for these two different simulated systems as well as for the experimental systems we studied in prior work.[29]

Comparing the two simulated systems (20-mers vs monomers), there is a notable difference in their apparent activation energies, evaluated at both constant volume, $E_V = (\partial(\ln \tau + \ln T^{1/2})/\partial T^{-1})_V$, and at constant pressure, $E_P = (\partial(\ln \tau + \ln T^{1/2})/\partial T^{-1})_P$. For example, at the same point, T = 1.0 and P = 3.0 in LJ units, the $E_V \approx 1.4$ and $E_P \approx 3.2$ values for the 20-mer melt are larger by about a factor of 2 compared to the corresponding $E_V \approx 0.65$ and $E_P \approx 1.6$ values for the monomeric KA−LJ fluid. This is partly connected to the observation (above) that the 20-mer melt has the larger activation energy per cooperating particle/segment. An even more important factor contributing to the difference is in how the 20-mer melt has lower relative free volume values compared to monomers; for example, at T = 1.0 and P = 3.0, V_{free}/V_{hc} = 0.20 for the 20-mers, while V_{free}/V_{hc} = 0.33 for the KA−LJ monomers. This implies that the polymer melt (at the same T, P) requires more cooperating particles/segments in order to rearrange, and this larger n^* $(\propto 1/V_{free})$ thus leads to higher $\Delta A_{act} = n^*\Delta a$.

Another interesting quantity to compare is the ratio of the apparent activation energies, E_V/E_P, which is a measure of a system's volume vs temperature sensitivity.[1,3] High values close to 1 indicate little sensitivity to changes in volume, and low values closer to 0 indicate strong sensitivity to changes in volume. When comparing experimental systems in the literature, the value of E_V/E_P is often taken at the system $T = T_g$ and P = 1 atm. Note that E_V/E_P values change with T, P (e.g., the ratio of slopes at the crossing points in Figure 7 are T, P-dependent), and we can analyze and compare these trends.

In Table 1, we show the E_V/E_P values at several different choices of T, P for both the simulated 20-mer polymer and the monomeric KA−LJ fluid. At all T, P points, the E_V/E_P values are consistently lower for the monomeric fluid compared to the 20-mer melt, which demonstrates the stronger sensitivity to volume change in the monomer fluid. This is consistent with tabulations for experimental systems (e.g., Table 2 of the

Table 1. Trends in the Ratio of Apparent Activation Energies (E_V/E_P)[a]

P	$1/T$	20-mer E_V/E_P	KA−LJ E_V/E_P
0.5	1.0	0.36	0.27
0.5	1.5	0.43	0.36
3.0	1.0	0.43	0.39
3.0	1.5	0.52	0.49

[a]The E_V/E_P results here correspond to the simulation results, though the corresponding CFV model values are similar. The E_V/E_P values were calculated by estimating $E_V = (\partial(\ln \tau + \ln T^{1/2})/\partial T^{-1})_V$ and $E_P = (\partial(\ln \tau + \ln T^{1/2})/\partial T^{-1})_P$ from the local slopes of the simulation data on isochores and isobars, respectively. Note that in the simulation data the isochores do not cross at the exact $1/T$ and P values listed in this table, and so weighted averages using the two closest isochores were used to estimate the E_V value. The estimated uncertainty in the E_V/E_P values is ±0.02.

DOI: 10.1021/acs.macromol.8b00591
Macromolecules 2018, 51, 4896−4909

Roland et al. review[1]) that show lower average E_V/E_P for small molecules compared to polymers. The results in Table 1 also demonstrate that for both simulated systems E_V/E_P increases with decreasing temperature (at fixed P), and it increases with increasing pressure (at fixed T). Note, also, that the monomeric fluid's E_V/E_P is affected more strongly than the 20-mer on going from low to higher pressure.

Trends in the T, P dependence of E_V/E_P have been reported (e.g., via dielectric spectroscopy) for some experimental systems in the literature. Examples include results from Floudas and co-workers for poly(2-vinylpyridine) (P2VP)[78] and poly(vinyl isobutyl ether) (PViBE)[79] and from Naoki et al.[80] for poly(vinyl chloride) (PVC) and the small molecule *o*-terphenyl (OTP). The trends in E_V/E_P for the experimental systems are diverse and system-specific. The small molecule, OTP, like the present simulation results, showed an increasing E_V/E_P with decreasing T, and so did P2VP. However, the opposite trend was observed for PViBE, and there was nonmonotone behavior for PVC. Most of the experimental systems showed an increase in E_V/E_P with increasing P, which is the same trend as for the present simulated systems. Note in addition that most of the experimental E_V/E_P values are higher than the average E_V/E_P values for the simulated systems in Table 1. This is likely because the simulated systems are probed at higher temperatures relative to system T_g.

In Figure 8, we highlight the range of applicability of eq 6 to the 20-mer fluid from an overall "*PVT* space perspective". We

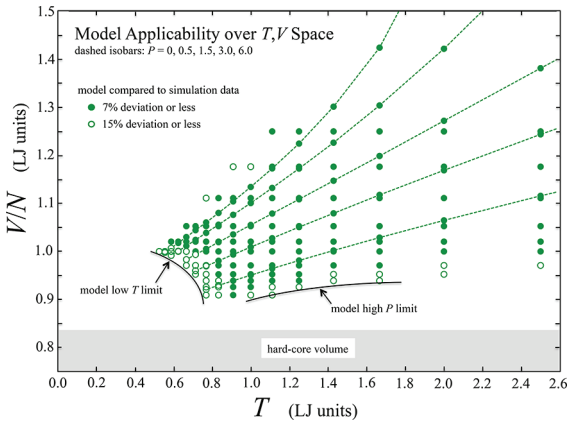

Figure 8. Range of the 20-mer fluid *PVT* space described by the CFV model eq 6. The symbols illustrate agreement between simulation and model over a range of *PVT* space. The quantity $[\ln \tau + \ln T^{1/2} - C_3]$ was calculated using the model τ, and using the simulation τ, and then compared. 7% deviation or less is indicated by solid symbols. 15% deviation or less is indicated by open symbols. The applicable *PVT* space encompasses T and V_{free} values that can each change by more than factor of 5, with relaxation times that can vary (depending on T and V_{free}) anywhere in the range of more than two base 10 orders of magnitude.

compare the model and simulation values for $[\ln \tau + \ln T^{1/2} - C_3]$; i.e., we calculate the value of $[\ln \tau + \ln T^{1/2} - C_3]$ using the model τ and compare it to the corresponding value calculated using the simulation τ value. A symbol is marked at each of the simulation T, V data points where the model results agreed to within a threshold of the simulation data. Satisfaction of two agreement criteria are marked: 15% deviation or less (open symbols) and 7% deviation or less (solid symbols). The model's "applicable region" thus appears visually as the scatter pattern of colored points spreading over the T, V space. As a guide, dashed lines identify the isobars, P = 0, 0.5, 1.5, 3.0, and 6.0.

The model shows good agreement with the simulation data through all of the T, V regions lying between the P = 0 and 6.0 isobars over a temperature interval that spans very high T (T = 5, beyond the plotted range) down to the model's low-T limit; the low-T and high-P bounds are roughly indicated in the figure. The more generous criterion, signifying agreement within 15%, brings in many points that extend outside the P = 0 and 6.0 isobars, including some located above the P = 0 isobar that are identified with negative pressures. The points that lie visually below the P = 6.0 isobar show that the model's high P limit extends up to pressures around 9 or 10 (and even 12 at the higher T's). A pressure of P = 9 in LJ units corresponds to almost 400 MPa for an argon-like fluid.

Though the simple eq 6 model cannot describe the low T regime, it is still striking how large the range of general applicability is in *PVT* space. Over the applicable range of eq 6, the input variables, T and V_{free}, each can vary by more than a factor of 5, and the resulting relaxation times will then vary in a detailed way (depending on the particular T and V_{free}) anywhere in the range of more than two base 10 orders of magnitude. As emphasized above, this regime of applicability includes an accurate description of the non-Arrhenius behavior on isobars, and this is noteworthy because eq 6 is based on the simplest imaginable assumption of a constant activation energy per cooperating segment (C_2).

We now turn to some thoughts on applying the CFV model at low T. In ref 29 we first deduced the low-T CFV form (eq 7, $\ln \tau = (V_{hc}/V_{free})(T^*/T)^b + \ln \tau_{ref}$) by applying arguments analogous to those in thermodynamic scaling approaches.[1,3,45−55] The resulting eq 7 indeed works very well in describing pressure-dependent dynamics over a range of low T near an experimental system's T_g; however, its T dependence cannot be correct in the high-T regime. Subsequent goals were to obtain a more physical explanation for understanding the source of the form $(1/V_{free}) \times f(T)$ and to capture the high-T range behavior that makes up such an important portion of the results in simulated glassy melts. These goals have been met through the derivation of eq 6. Because eq 6 gets all of the high-T behavior correct, particularly the volume contribution to non-Arrhenius behavior, it provides the formalism for connecting with eq 7.

A fundamental prediction that comes from the CFV derivation is the linearity of $\ln \tau$ vs $1/V_{free}$ on isotherms (and with slopes that increase with decreasing T). In *all* of the systems that we have studied to date, we find this behavior to hold at *all* T. For example, the clear linearity of the isotherms in Figure 4 is maintained at both high and low T (regardless of whether or not the simple eq 6 with constant C_2 applies). We draw the firm conclusion that any changes in the free energy of activation that are caused by changes in volume (fixed T) can be correctly described by the CFV framework of $\Delta A_{act} \propto n^* \propto 1/V_{free}$, from high T to low T.

Having determined that free volume is the natural variable for mapping data on dynamic relaxation, and particularly that the $1/V_{free}$ functional form applies as the volume contribution over all simulated/experimental parameter space, we then distinguish between two regimes in drawing conclusions about T dependence. When dealing with experimental systems, studied in temperature ranges close to T_g (say $T = T_g$ up to $\sim 1.3T_g$ or so) a simple empirical form (e.g., $\sim 1/T^b$, eq 7) applies. Equation 7 involves only three dynamics parameters,

DOI: 10.1021/acs.macromol.8b00591
Macromolecules 2018, 51, 4896−4909

and it can be used along any thermodynamic path through pressure-dependent relaxation space, yielding a description that is both practical and predictive (contrast with the three-parameter VFT equation, which cannot describe more than one single isobar or isochore). On the other hand, for the very broad T-range, shifted to higher temperatures and covering the Arrhenius to non-Arrhenius transition regime (commonly probed in simulated fluids), it is the form of eq 6 that very effectively captures the T-dependent behavior.

4. SUMMARY AND CONCLUSIONS

In this article we have applied the cooperative free volume (CFV) model to analyze and explain the pressure dependent dynamics, $\tau(T,V)$, for a simulated polymer melt in the high T and Arrhenius to non-Arrhenius transition regime.

The cooperative free volume model is based on the following: (1) The rate of relaxation is governed by an overall free energy of activation ($\Delta A_{act} = n^*\Delta a$) that increases with the number of cooperating segments (n^*). (2) The system's thermodynamic free volume ($V_{free} = V - V_{hc}$) is what determines n^*. For relaxation to occur, space needs to be made to allow the entry of a segment. Assuming that a cooperating group of nearby segments must contain, in total, some characteristic amount of free volume (in order to make that space) leads to the form, $n^* \propto 1/V_{free}$.

The relationships $\Delta A_{act} = n^*\Delta a$ and $n^* \propto 1/V_{free}$, together with the assumption of constant activation energy per cooperating segment, are the essentials that lead to the CFV model's form eq 6, $\ln \tau = C_1(V_{hc}/V_{free}) \times (1 + C_2/T) - \ln T^{1/2} + C_3$.

Equation 6 describes the pressure-dependent dynamics over a regime that spans Arrhenius to non-Arrhenius behavior. It matches the simulation data over a very wide range of the 20-mer fluid's T, V space, covering in particular the high- to mid-T range, a regime that is important in simulation studies. The form of the T dependence in eq 6 eventually breaks down at lower T as the system's glass transition temperature is approached; application in this lower T regime (e.g., typically probed by dielectric relaxation spectroscopy) requires the use of the related model eq 7. Equations 6 and 7 can both be derived starting from the same basic cooperative $\Delta A_{act} = n^*\Delta a$ and $n^* \propto 1/V_{free}$ structure,[73] and this leads to the general form $\ln \tau \sim (1/V_{free}) \times f(T)$, which works under all conditions, though the T contribution ($f(T)$) in eq 7 is empirical.

We note that as in our analysis of simulation data on monomers,[73] important features of eq 6 are that it reflects both an energetic and an entropic contribution to the activation free energy and a prefactor temperature dependence from the gas kinetic velocity. We have verified that all of these effects make a contribution in the 20-mer simulation data, and we believe this will be true in most simulation studies, which tend to probe glassy systems at a relatively high range of T.

Of course, use of this approach relies on our straightforward and unambiguous predictions for $V_{free}(T,P)$, which require only PVT data (experimental or simulated), and is carried out independently of the dynamics results. Note that knowing the form of the volume contribution ($\sim 1/V_{free}$) allows our expressions (eqs 6 and 7) to require only three dynamics parameters, while pressure-dependent descriptions typically require four. A case in point: the three-parameter VFT equation cannot express P-dependent dynamics.

One of the most important predictions that follows from the generalized CFV $\ln \tau \sim (1/V_{free}) \times f(T)$ functional form, and is shown clearly in the 20-mer results reported here, is that $\ln \tau$ vs inverse free volume ($1/V_{free}$) is linear on *isotherms*, with slopes that will increase with decreasing T. This has also been the case for all the earlier systems we have studied, including simulations of the KA–LJ monomeric fluid[73] and analysis of experimental data on polymeric and small molecule glass-formers.[29] As noted above, the conclusion is that the volume contribution for all systems can be effectively captured using the natural variable, $1/V_{free}$.

Turning to *isobars*, the CFV model reveals that a key source of non-Arrhenius behavior arises from the T dependence of V_{free}. As $1/V_{free}$ increases with $1/T$, the number of cooperating segments also increases ($n^* \propto 1/V_{free}$), which results in an increasing activation energy ($\Delta A_{act} = n^*\Delta a$). To our knowledge, an explanation such as this has never been presented before. Though the connection of V_{free} to activation energy is not the only source of non-Arrhenius behavior, it is the first source, important in the high-T regime, and it remains important at low T near T_g.

APPENDIX. MOLECULAR DYNAMICS SIMULATION DETAILS

In the following we describe the details for the molecular dynamics (MD) simulations. The polymer molecules are described by a bead–spring type of model that is commonly implemented in the literature.[62,63,74,74] We have followed the choices of model parameters in Mangalara and Simmons, who presented (see their Supporting Information)[63] a detailed description of the model and some corresponding average properties at $P = 0$, e.g., relaxation times and average volume and energy, and we have compared to their results to verify our own simulation results.

The interactions between all segments (beads) that are not directly bonded to each other are described by the Lennard-Jones potential, $u_{LJ}(r)$, given by

$$u_{LJ}(r) = 4\varepsilon[(\sigma/r)^{12} - (\sigma/r)^6] \quad \text{(A1)}$$

where r is the pair separation distance, and σ and ε are the LJ characteristic distance and energy parameters, respectively. The interactions between directly bonded segments are described by the finitely extensible nonlinear elastic (FENE) potential,[81,82] given by

$$u_{FENE}(r) = -0.5KR_0^2 \ln[1 - (r/R_0)^2] + 4\varepsilon[(\sigma/r)^{12} - (\sigma/r)^6] + \varepsilon \quad \text{(A2)}$$

where $K = 30$ and $R_0 = 1.5$. Note that the nonbonded u_{LJ} interaction includes attractions, while the in the bonded u_{FENE} interaction the LJ contribution is truncated at $r = 2^{1/6}\sigma$ and shifted to zero at this distance so as to be repulsive only.

In all cases the quantities are given in standard LJ units where length is in units of σ, energy in units of ε, time in units of $\sigma(m/\varepsilon)^{1/2}$, etc., where m is the mass. As noted in the main text, each linear polymer molecule is comprised by 20 segments, and the simulated system consisted of a total of $N = 1600$ segments (80 molecules). The molecular dynamics (MD) simulations were run under standard periodic boundary conditions and where the nonbonded pair interactions were cut off at a distance of $r = 2.5\sigma$ where the potential was truncated and shifted to zero. (This small energy shift was not written explicitly in eq A1.) There are no tail corrections in the average properties.

DOI: 10.1021/acs.macromol.8b00591
Macromolecules 2018, 51, 4896–4909

The MD trajectories were integrated using the velocity form of the Verlet algorithm.[83] The time step size was dt = 0.002. The main runs (data collection runs) were simulated in the canonical (N, V, T) ensemble using an Andersen type of temperature bath.[84] However, the temperature coupling was done in a way that allowed for long stretches ("blocks") of microcanonical (N, V, E) simulation, wherein at the beginning of a block all the atom velocities were replaced with a new set drawn from the Maxwell−Boltzmann distribution for that T. Then, microcanonical NVE simulation was run for the entire block. The amount of time defining the block was set at a target value (based on trends in equilibration, etc.) such that it would be at least 3 times the relaxation time (τ) for the particular conditions (and often, e.g., at higher T's, it was much longer). Relaxation times were measured over the course of each NVE block. In the case of obtaining data on isobars, first, isobaric (N, P, T) simulations were performed using a Berendsen type of pressure and temperature coupling.[85] The resulting average volume from these NPT runs was then used as the fixed volume value for the above-described NVT/NVE-type runs that followed, wherein the relaxation data were collected (and average pressure was verified to be the same as the original set pressure from the run with Berendsen-type coupling).

Relaxation times were calculated based on the self-intermediate scattering function, $F_s(q,t)$, which is a measure of the movement of a segment over time. It is given by

$$F_s(q, t) = (1/N)\langle \sum \exp[i\mathbf{q}\cdot(\mathbf{r}_j(t) - \mathbf{r}_j(0)]\rangle \quad \text{(A3)}$$

where the sum runs over all segments, j = 1 to N. As in ref 63, the value of $q = 7.07\sigma^{-1}$ was used to define the length scale, which is close to the value of the first peak in the structure factor. The relaxation time, τ, is defined to be the time when $F_s(q,t)$ has decayed to a value of 0.2.

Relaxation times were simulated for many points in the PVT space. The strategy for ordering and equilibrating the runs was to start from high temperatures and low densities, the same strategy described in our work on the KA−LJ monomeric system (see Appendix B of ref 73). Typically, the total production run lengths were carried out to 250 blocks and were equilibrated before that for 100 blocks. The density of the data points along with the general smoothness of the data trends is an indication of reasonably low uncertainties in the relaxation times. Taking the 250 block run at $1/T$ = 1.3 and N/V = 1.03 as an example, if each individual block is treated as a separate result for ln τ, then these 250 results had a standard deviation of 0.18, and the error in the average of these results (defined by the standard deviation of the mean) is thus about 0.011, which is smaller than the data point symbol size in Figure 4. Errors should be somewhat higher for points at lower T and higher density, though in general, we tried to limit our coverage to state points where we felt we could get reliable τ values.

AUTHOR INFORMATION

Corresponding Author

*E-mail: jane.lipson@dartmouth.edu (J.E.G.L.).

ORCID

Jane E. G. Lipson: 0000-0002-0177-9373

Notes

The authors declare no competing financial interest.

ACKNOWLEDGMENTS

We gratefully acknowledge the financial support provided by the National Science Foundation (DMR-1403757 and DMR-1708542) and the computational resources and support provided by the Research Computing group at Dartmouth College. J.E.G.L. also acknowledges the Radcliffe Institute for Advanced Study at Harvard University.

REFERENCES

(1) Roland, C.; Hensel-Bielowka, S.; Paluch, M.; Casalini, R. Supercooled dynamics of glass-forming liquids and polymers under hydrostatic pressure. *Rep. Prog. Phys.* **2005**, *68*, 1405−1478.

(2) Roland, C. M. Relaxation Phenomena in Vitrifying Polymers and Molecular Liquids. *Macromolecules* **2010**, *43*, 7875−7890.

(3) Floudas, G.; Paluch, M.; Grzybowski, A.; Ngai, K. *Molecular Dynamics of Glass-Forming Systems - Effects of Pressure*; Springer: Berlin, 2011.

(4) Floudas, G. *Broadband Dielectric Spectroscopy*; Springer: Berlin, 2003.

(5) Cangialosi, D. Dynamics and thermodynamics of polymer glasses. *J. Phys.: Condens. Matter* **2014**, *26*, 153101.

(6) Napolitano, S.; Glynos, E.; Tito, N. B. Glass transition of polymers in bulk, confined geometries, and near interfaces. *Rep. Prog. Phys.* **2017**, *80*, 036602.

(7) Stillinger, F. H.; Debenedetti, P. G. Glass Transition Thermodynamics and Kinetics. *Annu. Rev. Condens. Matter Phys.* **2013**, *4*, 263−285.

(8) Debenedetti, P. G.; Stillinger, F. H. Supercooled liquids and the glass transition. *Nature* **2001**, *410*, 259−267.

(9) Ediger, M.; Angell, C.; Nagel, S. Supercooled liquids and glasses. *J. Phys. Chem.* **1996**, *100*, 13200−13212.

(10) Angell, C.; Ngai, K.; McKenna, G.; McMillan, P.; Martin, S. Relaxation in glassforming liquids and amorphous solids. *J. Appl. Phys.* **2000**, *88*, 3113−3157.

(11) Angell, C.; Borick, S. Specific heats C-p, C-v, C-conf and energy landscapes of glassforming liquids. *J. Non-Cryst. Solids* **2002**, *307-310*, 393−406.

(12) Martinez, L. M.; Angell, C. A. A thermodynamic connection to the fragility of glass-forming liquids. *Nature* **2001**, *410*, 663−667.

(13) Ferrer, M.; Lawrence, C.; Demirjian, B.; Kivelson, D.; Alba-Simionesco, C.; Tarjus, G. Supercooled liquids and the glass transition: Temperature as the control variable. *J. Chem. Phys.* **1998**, *109*, 8010−8015.

(14) McKenna, G. B. A brief discussion: Thermodynamic and dynamic fragilities, non-divergent dynamics and the Prigogine-Defay ratio. *J. Non-Cryst. Solids* **2009**, *355*, 663−671.

(15) Mckenna, G. B.; Simon, S. L. Challenges in the Dynamics and Kinetics of Glass-Forming Polymers. *Macromolecules* **2017**, *50*, 6333−6361.

(16) Berthier, L.; Biroli, G. Theoretical perspective on the glass transition and amorphous materials. *Rev. Mod. Phys.* **2011**, *83*, 587−645.

(17) Dyre, J. C. Colloquium: The glass transition and elastic models of glass-forming liquids. *Rev. Mod. Phys.* **2006**, *78*, 953−972.

(18) Chen, K.; Saltzman, E. J.; Schweizer, K. S. Segmental dynamics in polymers: from cold melts to ageing and stressed glasses. *J. Phys.: Condens. Matter* **2009**, *21*, 503101.

(19) Vogel, H. The temperature dependence law of the viscosity of fluids. *Phys. Z.* **1921**, *22*, 645−646.

(20) Fulcher, G. S. Analysis of recent measurements of the viscosity of glasses. *J. Am. Ceram. Soc.* **1925**, *8*, 339−355.

(21) Tammann, G.; Hesse, W. The dependancy of viscosity on temperature in hypothermic liquids. *Z. Anorg. Allg. Chem.* **1926**, *156*, 245.

(22) Cohen, M. H.; Turnbull, D. Molecular Transport in Liquids and Glasses. *J. Chem. Phys.* **1959**, *31*, 1164−1169.

DOI: 10.1021/acs.macromol.8b00591
Macromolecules 2018, 51, 4896−4909

(23) Cohen, M. H.; Grest, G. S. Liquid-Glass Transition, a Free-Volume Approach. *Phys. Rev. B: Condens. Matter Mater. Phys.* **1979**, *20*, 1077−1098.
(24) Williams, M. L.; Landel, R. F.; Ferry, J. D. Mechanical Properties of Substances of High Molecular Weight 0.19. the Temperature Dependence of Relaxation Mechanisms in Amorphous Polymers and Other Glass-Forming Liquids. *J. Am. Chem. Soc.* **1955**, *77*, 3701−3707.
(25) Ferry, J. D. *Viscoelastic Properties of Polymers*; Wiley: New York, 1970.
(26) Adam, G.; Gibbs, J. H. On Temperature Dependence of Cooperative Relaxation Properties in Glass-Forming Liquids. *J. Chem. Phys.* **1965**, *43*, 139−146.
(27) Avramov, I. Pressure dependence of viscosity of glassforming melts. *J. Non-Cryst. Solids* **2000**, *262*, 258−263.
(28) Doolittle, A. K. Studies in Newtonian Flow 0.2. the Dependence of the Viscosity of Liquids on Free-Space. *J. Appl. Phys.* **1951**, *22*, 1471−1475.
(29) White, R. P.; Lipson, J. E. G. How Free Volume Does Influence the Dynamics of Glass Forming Liquids. *ACS Macro Lett.* **2017**, *6*, 529−534.
(30) Richert, R.; Angell, C. Dynamics of glass-forming liquids. V. On the link between molecular dynamics and configurational entropy. *J. Chem. Phys.* **1998**, *108*, 9016−9026.
(31) Prevosto, D.; Capaccioli, S.; Lucchesi, M.; Leporini, D.; Rolla, P. Pressure and temperature dependence of structural relaxation dynamics in polymers: a thermodynamic interpretation. *J. Phys.: Condens. Matter* **2004**, *16*, 6597−6608.
(32) Schwartz, G.; Tellechea, E.; Colmenero, J.; Alegria, A. Correlation between temperature-pressure dependence of the alpha-relaxation and configurational entropy for a glass-forming polymer. *J. Non-Cryst. Solids* **2005**, *351*, 2616−2621.
(33) Schwartz, G. A.; Colmenero, J.; Alegria, A. Pressure-temperature dependence of polymer segmental dynamics. comparison between the Adam-Gibbs approach and density scalings. *Macromolecules* **2006**, *39*, 3931−3938.
(34) Sciortino, F.; Kob, W.; Tartaglia, P. Inherent structure entropy of supercooled liquids. *Phys. Rev. Lett.* **1999**, *83*, 3214−3217.
(35) Sastry, S. The relationship between fragility, configurational entropy and the potential energy landscape of glass-forming liquids. *Nature* **2001**, *409*, 164−167.
(36) Berthier, L.; Coslovich, D. Novel approach to numerical measurements of the configurational entropy in supercooled liquids. *Proc. Natl. Acad. Sci. U. S. A.* **2014**, *111*, 11668−11672.
(37) Matsuoka, S.; Quan, X. A Model for Intermolecular Cooperativity in Conformational Relaxations Near the Glass-Transition. *Macromolecules* **1991**, *24*, 2770−2779.
(38) Adachi, K. A Molecular-Model for Cooperative Local Motions in Amorphous Polymers. *Macromolecules* **1990**, *23*, 1816−1821.
(39) Gotze, W.; Sjogren, L. Relaxation Processes in Supercooled Liquids. *Rep. Prog. Phys.* **1992**, *55*, 241−376.
(40) Gotze, W. Recent tests of the mode-coupling theory for glassy dynamics. *J. Phys.: Condens. Matter* **1999**, *11*, A1−A45.
(41) Schweizer, K.; Saltzman, E. Entropic barriers, activated hopping, and the glass transition in colloidal suspensions. *J. Chem. Phys.* **2003**, *119*, 1181−1196.
(42) Schweizer, K. Derivation of a microscopic theory of barriers and activated hopping transport in glassy liquids and suspensions. *J. Chem. Phys.* **2005**, *123*, 244501.
(43) Mirigian, S.; Schweizer, K. S. Unified Theory of Activated Relaxation in Liquids over 14 Decades in Time. *J. Phys. Chem. Lett.* **2013**, *4*, 3648−3653.
(44) Mirigian, S.; Schweizer, K. S. Dynamical Theory of Segmental Relaxation and Emergent Elasticity in Supercooled Polymer Melts. *Macromolecules* **2015**, *48*, 1901−1913.
(45) Casalini, R.; Roland, C. M. Thermodynamical scaling of the glass transition dynamics. *Phys. Rev. E* **2004**, *69*, 062501.
(46) Casalini, R.; Mohanty, U.; Roland, C. M. Thermodynamic interpretation of the scaling of the dynamics of supercooled liquids. *J. Chem. Phys.* **2006**, *125*, 014505.
(47) Casalini, R.; Roland, C. M. An equation for the description of volume and temperature dependences of the dynamics of supercooled liquids and polymer melts. *J. Non-Cryst. Solids* **2007**, *353*, 3936−3939.
(48) Alba-Simionesco, C.; Cailliaux, A.; Alegria, A.; Tarjus, G. Scaling out the density dependence of the a relaxation in glass-forming polymers. *Europhys. Lett.* **2004**, *68*, 58−64.
(49) Dreyfus, C.; Le Grand, A.; Gapinski, J.; Steffen, W.; Patkowski, A. Scaling the alpha-relaxation time of supercooled fragile organic liquids. *Eur. Phys. J. B* **2004**, *42*, 309−319.
(50) Ngai, K. L.; Habasaki, J.; Prevosto, D.; Capaccioli, S.; Paluch, M. Thermodynamic scaling of alpha-relaxation time and viscosity stems from the Johari-Goldstein beta-relaxation or the primitive relaxation of the coupling model. *J. Chem. Phys.* **2012**, *137*, 034511.
(51) Dyre, J. C. Hidden Scale Invariance in Condensed Matter. *J. Phys. Chem. B* **2014**, *118*, 10007−10024.
(52) Casalini, R.; Roland, C. M. Determination of the Thermodynamic Scaling Exponent for Relaxation in Liquids from Static Ambient-Pressure Quantities. *Phys. Rev. Lett.* **2014**, *113*, 085701.
(53) Puosi, F.; Chulkin, O.; Bernini, S.; Capaccioli, S.; Leporini, D. Thermodynamic scaling of vibrational dynamics and relaxation. *J. Chem. Phys.* **2016**, *145*, 234904.
(54) Bernini, S.; Puosi, F.; Leporini, D. Thermodynamic scaling of relaxation: insights from anharmonic elasticity. *J. Phys.: Condens. Matter* **2017**, *29*, 135101.
(55) Guo, J.; Simon, S. L. Thermodynamic scaling of polymer dynamics versus T - T-g scaling. *J. Chem. Phys.* **2011**, *135*, 074901.
(56) Casalini, R.; Capaccioli, S.; Lucchesi, M.; Rolla, P.; Corezzi, S. Pressure dependence of structural relaxation time in terms of the Adam-Gibbs model. *Phys. Rev. E: Stat. Phys., Plasmas, Fluids, Relat. Interdiscip. Top.* **2001**, *63*, 031207.
(57) White, R. P.; Lipson, J. E. G. Polymer Free Volume and Its Connection to the Glass Transition. *Macromolecules* **2016**, *49*, 3987−4007.
(58) Buchenau, U.; Zorn, R. A Relation between Fast and Slow Motions in Glassy and Liquid Selenium. *Europhys. Lett.* **1992**, *18*, 523−528.
(59) Starr, F.; Sastry, S.; Douglas, J.; Glotzer, S. What do we learn from the local geometry of glass-forming liquids? *Phys. Rev. Lett.* **2002**, *89*, 125501.
(60) Larini, L.; Ottochian, A.; De Michele, C.; Leporini, D. Universal scaling between structural relaxation and vibrational dynamics in glass-forming liquids and polymers. *Nat. Phys.* **2008**, *4*, 42−45.
(61) Betancourt, B. A. P.; Hanakata, P. Z.; Starr, F. W.; Douglas, J. F. Quantitative relations between cooperative motion, emergent elasticity, and free volume in model glass-forming polymer materials. *Proc. Natl. Acad. Sci. U. S. A.* **2015**, *112*, 2966−2971.
(62) Simmons, D. S.; Cicerone, M. T.; Zhong, Q.; Tyagi, M.; Douglas, J. F. Generalized localization model of relaxation in glass-forming liquids. *Soft Matter* **2012**, *8*, 11455−11461.
(63) Mangalara, J. H.; Simmons, D. S. Tuning Polymer Glass Formation Behavior and Mechanical Properties with Oligomeric Diluents of Varying Stiffness. *ACS Macro Lett.* **2015**, *4*, 1134−1138.
(64) Kob, W.; Andersen, H. C. Scaling Behavior in the Beta-Relaxation Regime of a Supercooled Lennard-Jones Mixture. *Phys. Rev. Lett.* **1994**, *73*, 1376−1379.
(65) Kob, W.; Andersen, H. C. Testing Mode-Coupling Theory for a Supercooled Binary Lennard-Jones Mixture - the Van Hove Correlation-Function. *Phys. Rev. E: Stat. Phys., Plasmas, Fluids, Relat. Interdiscip. Top.* **1995**, *51*, 4626−4641.
(66) Berthier, L.; Tarjus, G. Nonperturbative Effect of Attractive Forces in Viscous Liquids. *Phys. Rev. Lett.* **2009**, *103*, 170601.
(67) Berthier, L.; Tarjus, G. The role of attractive forces in viscous liquids. *J. Chem. Phys.* **2011**, *134*, 214503.
(68) Coslovich, D.; Roland, C. M. Thermodynamic scaling of diffusion in supercooled Lennard-Jones liquids. *J. Phys. Chem. B* **2008**, *112*, 1329−1332.
(69) Coslovich, D.; Roland, C. M. Pressure-energy correlations and thermodynamic scaling in viscous Lennard-Jones liquids. *J. Chem. Phys.* **2009**, *130*, 014508.

DOI: 10.1021/acs.macromol.8b00591
Macromolecules 2018, 51, 4896−4909

(70) Pedersen, U. R.; Bailey, N. P.; Schroder, T. B.; Dyre, J. C. Strong pressure-energy correlations in van der waals liquids. *Phys. Rev. Lett.* **2008**, *100*, 015701.
(71) Pedersen, U. R.; Schroder, T. B.; Dyre, J. C. Repulsive Reference Potential Reproducing the Dynamics of a Liquid with Attractions. *Phys. Rev. Lett.* **2010**, *105*, 157801.
(72) Sastry, S.; Debenedetti, P.; Stillinger, F. Signatures of distinct dynamical regimes in the energy landscape of a glass-forming liquid. *Nature* **1998**, *393*, 554−557.
(73) White, R. P.; Lipson, J. E. G. Explaining the T,V-dependent dynamics of glass forming liquids: The cooperative free volume model tested against new simulation results. *J. Chem. Phys.* **2017**, *147*, 184503.
(74) Starr, F. W.; Douglas, J. F.; Sastry, S. The relationship of dynamical heterogeneity to the Adam-Gibbs and random first-order transition theories of glass formation. *J. Chem. Phys.* **2013**, *138*, 12A541.
(75) As a check on our V_{hc} = 0.84 value, we have made isothermal ln τ vs V_{hc}/V_{free} plots assuming hypothetical values of V_{hc} = 0.83 and 0.85 (which are also reasonable looking *PVT*-based estimates). All of the values, 0.83, 0.84, and 0.85, lead to linear isotherms, just as we found in similar tests in ref 73. Furthermore, we have also verified how any hypothetical V_{hc} values that would not seem reasonable (visually), based on *PVT* analysis, do not lead to linear plots; values that are clearly too low (high) will result in strong positive (negative) curvature. See section II and Appendix A in ref 73 for a detailed analysis and comparison of plots for the case of the KA−LJ monomeric fluid.
(76) The uncertainty in C_2 of ± 0.3 means that there is about 7% resolution in weighting the relative strength of the energy of activation to that of the entropy of activation. Note that the product, C_1C_2 (as well as $C_1T + C_1C_2 \propto \Delta a$), is far more resolved (less variable) as a system-dependent quantity compared to C_2, as any change/uncertainty in the C_2 value (from visual assessment of data collapse) will always result (after linear fitting) in a C_1 value that compensates. For simplicity, we refer to the "activation energy per cooperating particle" as being proportional to C_2, though it is also proportional to the product C_1C_2; both are constants in eq 6 of course.
(77) Of course, the LJ interaction is not truly a hard sphere as infinite T is approached. The effect of the LJ repulsive core will be important as it lingers into very high T but will eventually be penetrable at extremely high T.
(78) Papadopoulos, P.; Peristeraki, D.; Floudas, G.; Koutalas, G.; Hadjichristidis, N. Origin of glass transition of poly(2-vinylpyridine). A temperature- and pressure-dependent dielectric spectroscopy study. *Macromolecules* **2004**, *37*, 8116−8122.
(79) Mpoukouvalas, K.; Floudas, G.; Verdonck, B.; Du Prez, F. Pressure-enhanced dynamic heterogeneity in block copolymers of poly(methyl vinyl ether) and poly(isobutyl vinyl ether). *Phys. Rev. E* **2005**, *72*, 011802.
(80) Naoki, M.; Endou, H.; Matsumoto, K. Pressure Effects on Dielectric-Relaxation of Supercooled Ortho-Terphenyl. *J. Phys. Chem.* **1987**, *91*, 4169−4174.
(81) Kremer, K.; Grest, G. Dynamics of Entangled Linear Polymer Melts - a Molecular-Dynamics Simulation. *J. Chem. Phys.* **1990**, *92*, 5057−5086.
(82) Grest, G.; Kremer, K. Molecular-Dynamics Simulation for Polymers in the Presence of a Heat Bath. *Phys. Rev. A: At., Mol., Opt. Phys.* **1986**, *33*, 3628−3631.
(83) Swope, W. C.; Andersen, H. C.; Berens, P. H.; Wilson, K. R. A Computer-Simulation Method for the Calculation of Equilibrium-Constants for the Formation of Physical Clusters of Molecules - Application to Small Water Clusters. *J. Chem. Phys.* **1982**, *76*, 637−649.
(84) Andersen, H. C. Molecular-Dynamics Simulations at Constant Pressure And-Or Temperature. *J. Chem. Phys.* **1980**, *72*, 2384−2393.
(85) Berendsen, H. J. C.; Postma, J. P. M.; van Gunsteren, W. F.; Dinola, A.; Haak, J. R. Molecular-Dynamics with Coupling to an External Bath. *J. Chem. Phys.* **1984**, *81*, 3684−3690.

DOI: 10.1021/acs.macromol.8b00591
Macromolecules 2018, 51, 4896−4909